

# Phonon Localization and a Boson-Peak-Like Anomaly in Twisted Penta-PdSe<sub>2</sub> Bilayer

Chenxin Zhang, Yanyan Chen, Qian Wang,\* and Puru Jena

Cite This: <https://doi.org/10.1021/acs.nanolett.5c01621>

Read Online

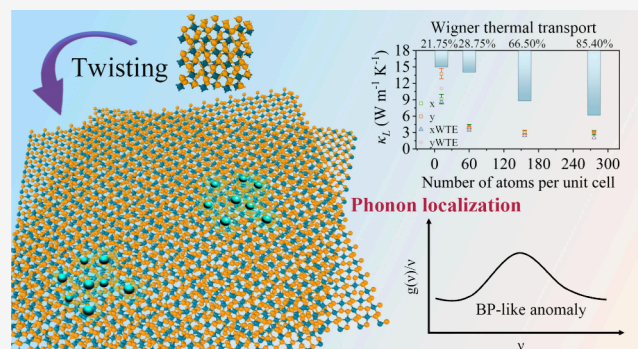
ACCESS |

Metrics & More

Article Recommendations

Supporting Information

**ABSTRACT:** With the emergence of twistronics, twisting has been employed to manipulate phonon–phonon interactions in 2D-layered systems. However, due to the complexity of twisted structures, twisting-induced phonon localization and Boson-peak-like (BP-like) anomalies have not yet been reported. In this work, using machine-learning-supported molecular dynamics, we study the impact of interlayer twisting on the phonon properties in bilayer pentagonal PdSe<sub>2</sub> (penta-PdSe<sub>2</sub>) with multiple twist angles. We find that twisting reduces the in-plane thermal conductivity by up to 78.62%, while significantly enhancing the phonon coherent thermal conductivity contribution from 21.75% to 85.40%. Furthermore, by analyzing the vibrational density of states and localized shear strain distribution, we demonstrate that twisting introduces the inhomogeneous shear modulus distribution, causing



phonon localization and a BP-like anomaly in twisted penta-PdSe<sub>2</sub> bilayers. These findings show that twisting becomes a new variable for producing a BP-like anomaly, different from the conventional strategies by using disorder, defects, or doping.

**KEYWORDS:** pentagonal sheet, twisting, Wigner transport, machine-learning potential, Boson-peak-like anomaly

It is of current interest to modulate the geometric structure and stacking configurations of 2D materials for effectively tuning the interatomic interactions and thermal conductivity ( $\kappa_L$ ).<sup>1</sup> For instance, introducing tensile strain in 2D structures can regulate their geometry and high-order scattering, leading to significant variation in lattice thermal conductivity.<sup>2,3</sup> Heterostacking-induced superlattices can suppress interlayer thermal conductivity, achieving ideal thermal insulators.<sup>4–6</sup> The pioneering study on magic-angle graphene by Cao et al. has fueled the development of twistronics,<sup>7,8</sup> further inspiring research on twist-modulated thermal conductivity in 2D materials. For example, interlayer twisting can significantly reduce in-plane thermal conductivity and enhance coherent thermal transport,<sup>9,10</sup> serving as an effective strategy for tuning phonon transport in 2D materials.

Recently, a Boson-peak-like (BP-like) anomaly<sup>11,12</sup> has been observed in some 2D-disordered and -layered van der Waals materials, such as vitreous 2D silica<sup>13</sup> and crystalline InSe,<sup>14</sup> where the coupling between out-of-plane (ZA) phonon modes and in-plane phonon modes leads to deviations from the Debye law in low-temperature heat capacity or excess vibrations in the phonon vibrational density of states (VDOS). Schirmacher et al.<sup>13,15–17</sup> conducted systematic studies on the Boson peak in disordered materials and attributed its emergence to the heterogeneous elasticity enhanced by disorder, distinguishing it from the van Hove singularities found in simple crystals. Notably, twisting can

enhance anharmonicity and reduce the lattice symmetry, thereby causing phonon localization,<sup>18,19</sup> which would induce a BP-like anomaly for manipulating thermal transport.

Among various 2D materials, pentagonal PdSe<sub>2</sub> (penta-PdSe<sub>2</sub>), the first experimentally synthesized pentagonal 2D material,<sup>20</sup> has shown great potential for applications in transistors,<sup>21</sup> thermoelectric applications,<sup>22</sup> and polarized photodetection<sup>23</sup> due to its unique geometric structure, high carrier mobility,<sup>21</sup> low thermal conductivity,<sup>24</sup> and distinctive optical properties,<sup>25</sup> which has significantly promoted the synthesis of other pentagonal 2D materials.<sup>26–28</sup> Theoretically, using the nonequilibrium Green's function method, Prasongkit et al.<sup>29</sup> reported that penta-PdSe<sub>2</sub> bilayers with twist angles of 37.7° and 90.0° show enhanced thermoelectric performance. However, the BP-like anomaly and phonon transport in such twisted bilayers were not explored. In this work, using machine-learning-supported molecular dynamics (MD)<sup>30,31</sup> with spectral energy density (SED)<sup>32,33</sup> analysis and Wigner transport theory,<sup>34</sup> we systematically investigate the phonon

**Received:** March 12, 2025

**Revised:** May 5, 2025

**Accepted:** May 5, 2025

response to interlayer twisting, the resulting BP-like anomalies, the underlying mechanisms, and the impact on lattice thermal conductivity.

We have generated 91 twisted structures of the bilayer penta-PdSe<sub>2</sub> by matching the common lattice vectors using the *CellMatch* package<sup>35</sup> and selected three structures with twist angles of 36.87°, 22.62°, and 41.13° for further study because they contain a smaller number of atoms (60, 156, and 276 atoms, respectively) in their unit cells. The schematic diagram and optimized atomic configurations of the three structures are presented in Figure 1. The detailed parameters of selected

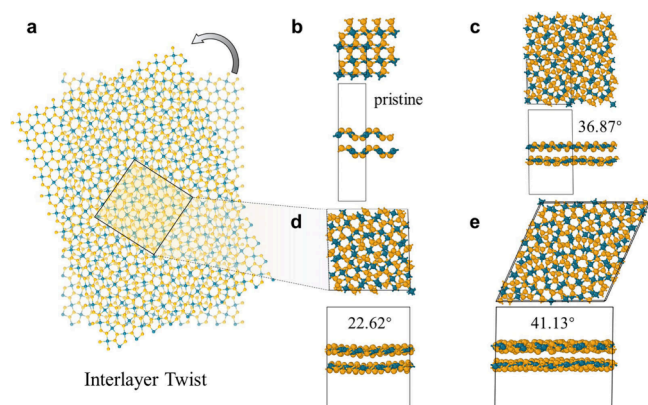


**Figure 1.** (a) Schematic diagram of the interlayer twist in a penta-PdSe<sub>2</sub> bilayer. (b–e) Top and side views of the geometric structures of a pristine penta-PdSe<sub>2</sub> bilayer and the twisted structures with angles of 36.87°, 22.62°, and 41.13°, respectively.

lattices are given in Table S1, which are consistent with previous studies.<sup>20,36</sup> The untwisted pristine bilayer sheet has a *Pca21* (No. 29) symmetry, while the symmetry of twisted structures is reduced to *P1* due to the complex stacking. The calculated harmonic phonon spectra of the selected structures are plotted in Figure S1, which shows no imaginary phonon frequencies, confirming that they are dynamically stable.

Parts b–e of Figure 1 show that, with increasing lattice complexity induced by twisting, the geometric anisotropy of the pristine sheet is significantly reduced in the twisted systems. In addition, a certain out-of-plane undulation is observed in the optimized twisted structures, as is the case with twisted bilayer graphene,<sup>37</sup> originating from the in-plane stress concentration induced by twisting. The resulting stress affects the mechanical properties and lattice anharmonicity.

Next, we investigated the thermal transport properties of the selected structures by calculating their lattice thermal conductivity using the homogeneous nonequilibrium molecular dynamics (HNEMD) method implemented in the *GPUMD* package,<sup>30,38</sup> combined with our neuroevolution potential [NEP; see details in the Supporting Information (SI)].<sup>31,39</sup> The results are listed in Figure 2a. The lattice thermal conductivities of the pristine system along the *x* and *y* directions are  $9.13 \pm 0.87$  and  $13.76 \pm 0.93$  W m<sup>-1</sup> K<sup>-1</sup>, respectively, exhibiting significant anisotropy, which are consistent with previous experimental results,<sup>24,40</sup> thus validating the accuracy of our NEP model. When twisting is applied, the thermal conductivities of twisted structures are significantly reduced compared to those of the pristine structure and monotonically decrease with the increased number of atoms in the twisted unit cell. For instance, the lattice thermal conductivities of twisted penta-PdSe<sub>2</sub> with a

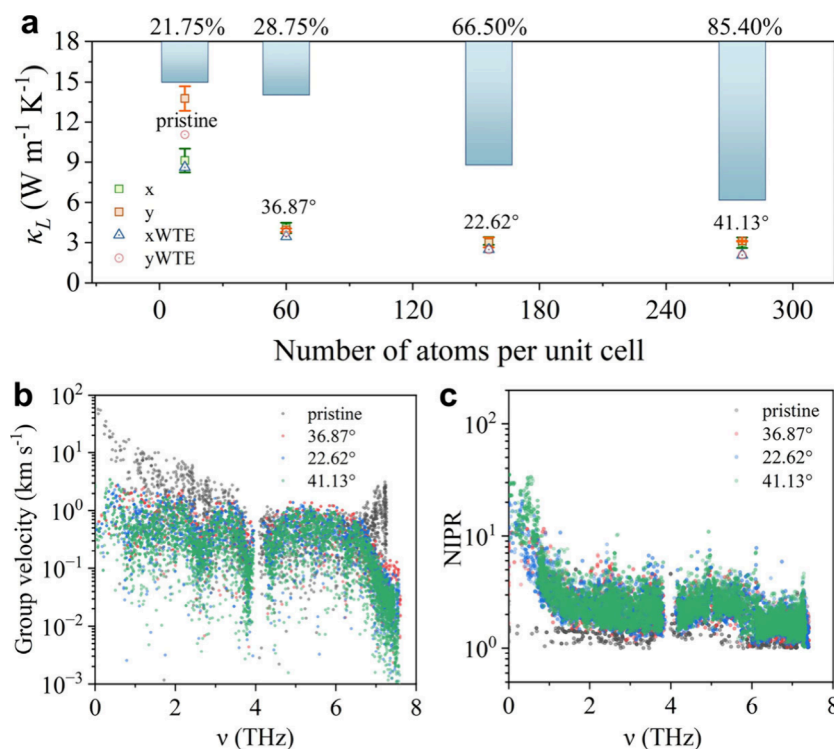


**Figure 2.** (a) Variation of the lattice thermal conductivity ( $\kappa_L$ ) with the number of atoms in the unit cell for different penta-PdSe<sub>2</sub> structures at 300 K. The bar charts represent the contribution ratio of phonon coherence to the lattice thermal conductivity. (b) Group velocities and (c) NIPR<sub>q</sub> as a function of the phonon frequency.

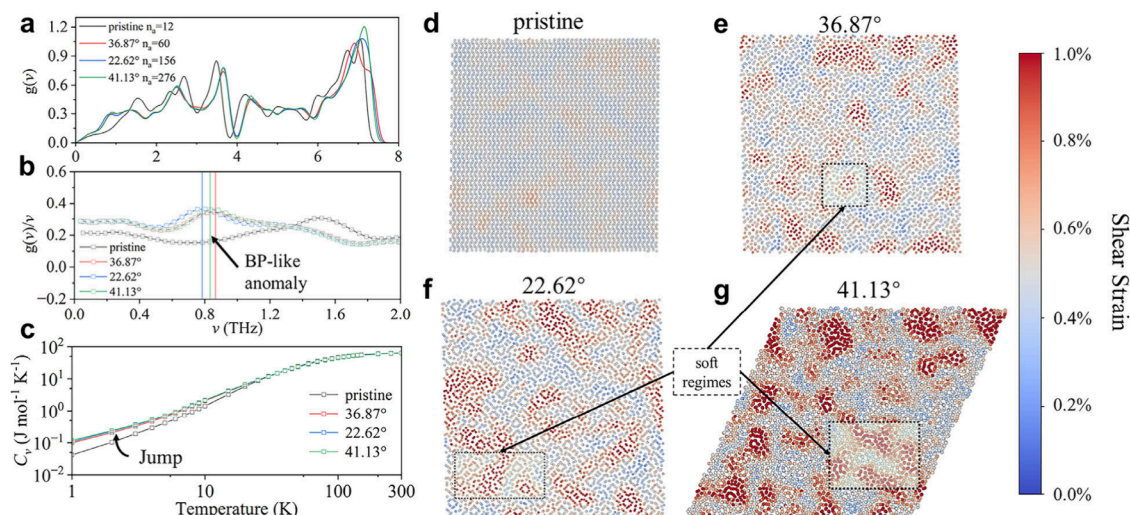


**Figure 3.** Evidence of the observed BP-like anomaly in twisted penta-PdSe<sub>2</sub>. (a) Calculated VDOS [ $g(\nu)$ ], (b) reduced VDOS [ $g(\nu)/\nu$ ], where the peaks of BP-like humps are marked by colored lines, and (c) variation of the calculated heat capacity with temperature. All results are normalized by the number of atoms per unit cell. (d–g) Localized shear strain distribution for the pristine and twisted structures under a 1.0% overall shear strain, with dashed rectangles marking the soft regimes within the twisted structures.

twist angle of  $41.13^\circ$  are only  $2.98 \pm 0.41$  and  $3.11 \pm 0.03$  W  $m^{-1} K^{-1}$  in the  $x$  and  $y$  directions at 300 K, respectively, which are only about 30% of the thermal conductivities of the pristine one (see details in Figure S2). It is worth noting that twisting weakens the anisotropy in the thermal transport properties of the twisted penta-PdSe<sub>2</sub>.

By using the phonon linewidth information ( $\Gamma_{q_i} = 1/\tau_{q_i}$ ) obtained from the SED method,<sup>32,33</sup> we calculate the lattice thermal conductivity of the selected systems using the Wigner transport equation (WTE) proposed by Simoncelli et al. (see details in the SI).<sup>34,41</sup> The results are compared with those obtained from the HNEMD method, achieving good consistency. Figure 2a shows the calculated contribution from the phonon coherence to the total lattice thermal conductivity of the penta-PdSe<sub>2</sub> systems with different twist angles, which results from the superposition of multiple phonon modes in a coordinated manner of wave-like excitations. Obviously, with increasing lattice complexity induced by the twist angle, the contribution of phonon coherence increased from 21.75% to 85.40%, gradually dominating the thermal transport properties of the twisted penta-PdSe<sub>2</sub> structures. According to eq S3, one can see that the materials with small frequency intervals and large phonon linewidths can exhibit stronger phonon coherence. As discussed in our previous work,<sup>9,10,42</sup> when the phonon linewidth is larger than the average frequency interval ( $\Delta\nu_{ave} = \nu_{max}/3n_a$ , where  $n_a$  is the number of atoms and  $\nu_{max}$  is the maximum frequency of phonon modes), the phonon modes contribute more to the phonon coherence than phonon scattering. As shown in Figure S3, the pristine and  $36.87^\circ$  structures have a lower ratio of phonon modes with linewidths larger than  $\Delta\nu_{ave}$ , resulting in a smaller contribution from phonon coherence. However, in the  $22.62^\circ$  and  $41.13^\circ$  twisted systems, there are extremely small  $\Delta\nu_{ave}$  values along with the significantly enhanced  $\Gamma_{q_i}$ , which suppress the propagation of phonons and enhance the contributions from coherence.

To explain the enhanced lattice anharmonicity and coherence induced by twisting, we calculated the phonon group velocities for all studied penta-PdSe<sub>2</sub> structures, as shown in Figure 2b. The results reveal a significant reduction

in the group velocities of low-frequency phonons, particularly the acoustic phonons, declining as the complexity of the twisted structures increases, which is also confirmed with the dynamic structure factor (DSF; see details in the SI) presented in Figure S3. This behavior differs from that of pentagonal graphene with lower anharmonicity.<sup>10</sup> The reduction in the group velocities of acoustic phonons leads to a decrease in lattice thermal conductivity. The calculated absolute value of the coherent thermal conductivity ( $\kappa_L^C$ ) and the contribution from the coherent phonon modes are plotted in Figure S4, which shows that  $\kappa_L^C$  of the twisted structures is lower than that of the pristine structure due to the decrease in their group velocities, consistent with our previous study on quasi-one-dimensional BiI<sub>3</sub>.<sup>42</sup> More importantly, as the complexity of the twisted structures increases, there are more nondegenerate coherent modes contributing to thermal transport (Figure S4b–e), thus leading to an increase in both the absolute value and the contribution ratio of  $\kappa_L^C$ .

For better understanding the results, we further calculate the normalized inverse participation ratio (NIPR<sub>q</sub>)<sup>43,44</sup> for measuring the degree of phonon localization, defined as

$$NIPR_q = n_a \sum_{i=1}^{n_a} \left( \sum_{\alpha} \varepsilon_{q_i\alpha}^2 \right)^2 \quad (1)$$

where  $\varepsilon_{q_i\alpha}$  is the eigenvector of a phonon mode  $\mathbf{q}$ ,  $n_a/NIPR_q$  represents the number of participating atoms in the motion of phonon  $\mathbf{q}$ . The larger the  $NIPR_q$  the more localized the phonon. As illustrated in Figure 2c, the  $NIPR_q$  values for low-frequency phonons in twisted structures increase significantly, indicating a substantial enhancement in the localization of phonon modes, due to the enhanced anharmonicity and reduced symmetry.<sup>19</sup>

Based on the atoms participation in the localized low-frequency phonon modes ( $NIPR_q > 20$ ) for the  $22.62^\circ$  and  $41.13^\circ$  cases, we find that string-like configurations contribute to the localized vibrations, consistent with previous studies on 2D glass,<sup>45</sup> as shown in Figure S5. Considering the significant decrease in the low-frequency phonon group velocity and these string-like configurations, it is likely that a BP-like anomaly will

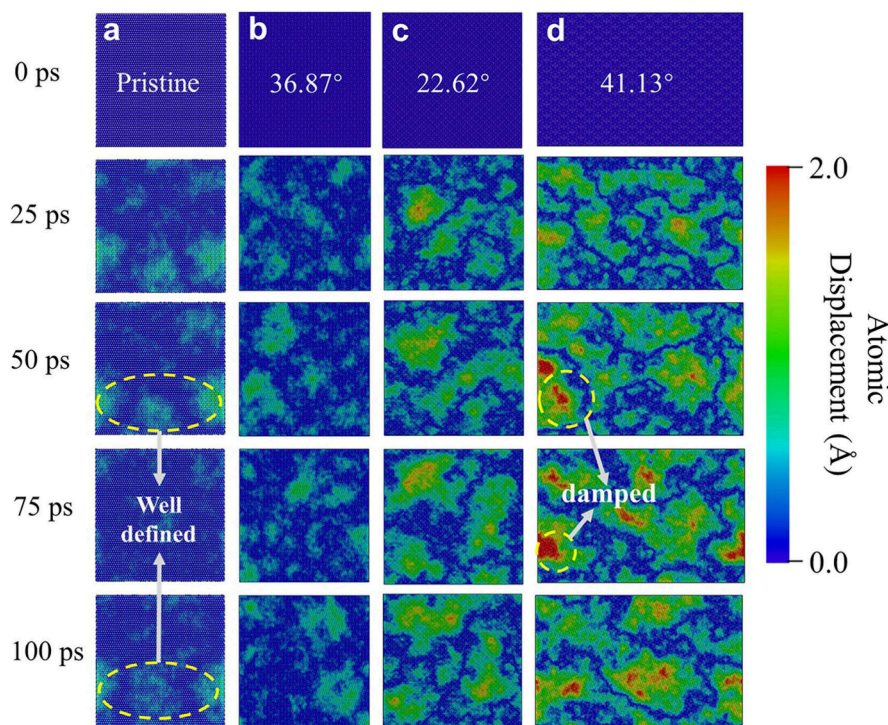


**Figure 4.** (a–d) Top view of atomic displacement fields from MD simulation of the pristine and twisted penta-PdSe<sub>2</sub> structures at the BP-like anomaly excitation temperature ( $\sim 40$  K). The atomic displacement distributions are 0, 25, 50, 75, and 100 ps from top to bottom. The yellow dashed circles highlight the features of atomic displacement corresponding to the low-frequency phonon modes.

be induced in the low-frequency region<sup>46</sup> and affect its transport properties. Therefore, we calculate the renormalized phonon VDOS [ $g(\nu)$ ] and the reduced VDOS [ $g(\nu)/\nu$ ] using the trained NEP potential and the Large-scale Atomic/Molecular Massively Parallel Simulator (LAMMPS) package,<sup>47</sup> combined with the renormalized phonon method implemented in the *DynaPhoPy* package.<sup>32</sup> The calculated results are plotted in Figure 3a,b.

As expected, we do find a BP-like anomaly in the low-frequency region (below  $\nu = 1$  THz) in these twisted structures, which can be clearly seen in Figure 3b. Except for the reduced VDOS curve of the pristine bilayer penta-PdSe<sub>2</sub>, each curve of the twisted structures has a convex peak in its low-frequency region. We further calculated the heat capacities of the selected systems. The calculated results, as plotted in Figure 3c, show that there is a characteristic jump in the low-temperature region below 10 K. This evidence confirms that the BP-like anomaly can be induced by introducing interlayer twisting in 2D bilayers.

To reveal the origin of the BP-like anomaly in twisted systems, we use heterogeneous elasticity theory (HET),<sup>13,17</sup> which has proven to be more accurate in describing the BP-like anomaly. The core idea is that an inhomogeneous shear modulus distribution in materials leads to phonon localization and the accumulation of additional modes, defined as

$$G_{xy}(\mathbf{r}) = G_{xy,0} + \Delta G_{xy}(\mathbf{r}) \quad (2)$$

where  $G_{xy,0}$  is the overall shear modulus and  $\Delta G_{xy}(\mathbf{r})$  represents the additional spatially random distribution. As shown in Figure 3d–g, when the overall shear strain is applied, the atomic strain in the pristine structure is uniformly distributed. However, soft regimes with random distribution appear in twisted systems and become more pronounced as the

twist-induced complexity increases. These HET-based results prove that twisting leads to phonon localization and BP-like anomalies caused by the inhomogeneous elasticity.

To further demonstrate that the twisting-induced inhomogeneous mechanical properties can cause the BP-like hump and enhance phonon localization, we used MD simulations to analyze atomic motions near the excitation temperature of the BP-like hump. We plot atomic displacement fields for 100 ps in Figure 4, showing that the atomic displacements in pristine penta-PdSe<sub>2</sub> exhibit periodic characteristics over time, reflecting well-defined phonon modes, as highlighted with yellow circles in Figure 4a; more details are given in Figure S6. However, in the twisted structures, particularly in the most complex one, as shown with yellow circles in Figure 4d, an accumulation of atomic displacement exists. This results in diffusive behavior as the atomic displacements slowly spread beyond the local region over time, losing their periodic characteristics. Due to the phonon linewidths over the Ioffe–Regel limit,<sup>34,48</sup> as shown in Figure S3, induced by the heterogeneous elasticity, phonons can hardly propagate to other regions. This provides an atomic-scale explanation for why coherent thermal transport dominates in twisted structures.

To further understand the impact of twisting on phonon transport, we discuss phonon damping in the twisted structures through a detailed analysis of phonon interactions. We compute the eigenvectors of the dynamical matrices for both pristine and twisted systems and plot the modulus of the matrix elements at the  $\mathbf{q}$  point near the Brillouin zone center along the [100] direction, as shown in Figure S7, where the  $x$  axis represents the atomic index in the unit cell and the  $y$  axis represents the vibrational modes in the sequence of low-to-high frequency. Both axes have  $3n_a$  elements. Each row corresponds to a vibrational mode, and every three columns

represent the vibrations of an atom in three directions, respectively. The color of each element block indicates the amplitude of the vibration. By comparing the lowest-frequency vibrations of the first four Pd atoms in the atomic index as examples of the pristine structure with those in the twisted structures in Figure S7, one can see that the clear distinction between the ZA and in-plane transverse acoustic (TA) modes in the pristine structure becomes blurred upon interlayer twisting. Significant coupling occurs in the 22.62° and 41.13° twisted structures, as shown in Figure S7b,d. According to Figure S3, the response of the ZA modes along the [110] direction becomes more and more obvious as the complexity of the twisted structure increases, further confirming that the coupling between the ZA and TA modes is enhanced with the interlayer twist. The coupling between the acoustic modes leads to significant phonon damping effects in the low-frequency region in the 41.13° twisted structure, as shown in Figure 4d.

In summary, by employing machine-learning-potential-based MD simulations combined with SED analysis and the WTE, we carry out detailed studies on the phonon properties of twisted penta-PdSe<sub>2</sub> bilayer sheets with different twisting angles. We have found that the lattice anharmonicity and coherent phonon transport in the twisted systems are significantly enhanced. Through anharmonic VDOS and localized shear strain distribution calculations, we have demonstrated that the interlayer twisting introduces an inhomogeneous elastic distribution (random localization of shear modulus) in the bilayer structure, leading to stronger coupling between the ZA and TA modes, enhancing the anharmonicity and localization of phonon modes, and thus inducing the BP-like hump in twisted penta-PdSe<sub>2</sub>. Meanwhile, the enhanced low-frequency phonon coupling and phonon localization with increased phonon linewidths lead to phonon overdamping. This study provides theoretical insights into the impact of interlayer twisting on phonon localization and BP-like anomaly.

## ■ ASSOCIATED CONTENT

### SI Supporting Information

The Supporting Information is available free of charge at <https://pubs.acs.org/doi/10.1021/acs.nanolett.5c01621>.

Methods, additional data and figures, including the details of first-principles calculations, Wigner thermal transport, homogeneous nonequilibrium MD simulations, DSF calculations and training of machine-learning potential, information on twisted penta-PdSe<sub>2</sub> structures, phonon spectra of all selected structures, detailed results of HNEMD simulations, calculated DSF and phonon linewidths, phonon coherent thermal conductivity and the contributions from coherent modes, top views of the string-like atomic structures contributing to localized phonon modes, three-dimensional trajectory curves of selected atoms in the pristine structure and average lifetimes of corresponding phonons, normalized modulus of eigenvector elements of dynamical matrices indexed by the order of atoms and phonon modes, training accuracy of the NEP model, and comparison between the mass-normalized velocity autocorrelation functions of AIMD and HNEMD simulations (PDF)

## ■ AUTHOR INFORMATION

### Corresponding Author

Qian Wang – School of Materials Science and Engineering, Peking University, Beijing 100871, China; [orcid.org/0000-0002-9766-4617](https://orcid.org/0000-0002-9766-4617); Email: [qianwang2@pku.edu.cn](mailto:qianwang2@pku.edu.cn)

### Authors

Chenxin Zhang – School of Materials Science and Engineering, Peking University, Beijing 100871, China

Yanyan Chen – School of Materials Science and Engineering, Peking University, Beijing 100871, China

Puru Jena – Department of Physics, Virginia Commonwealth University, Richmond, Virginia 23284, United States; [orcid.org/0000-0002-2316-859X](https://orcid.org/0000-0002-2316-859X)

Complete contact information is available at:

<https://pubs.acs.org/doi/10.1021/acs.nanolett.5c01621>

### Notes

The authors declare no competing financial interest.

## ■ ACKNOWLEDGMENTS

This work is partially supported by a grant from the National Natural Science Foundation of China (Grant NSFC-12274007) and is also supported by the High-Performance Computing Platform of Peking University, China. C.Z. thanks Y. H. Li and N. J. Liang for helpful discussions. P.J. acknowledges partial support by the U.S. Department of Energy, Office of Basic Energy Sciences, Division of Materials Sciences and Engineering, under Award DE-FG02-96ER45579.

## ■ REFERENCES

- (1) Liu, Y.; Jin, L.; Pandey, T.; Sun, H.; Liu, Y.; Li, X.; Rodriguez, A.; Wang, Y.; Zhou, T.; Chen, R.; Sun, Y.; Yang, Y.; Chrzan, D. C.; Lindsay, L.; Wu, J.; Yao, J. Anomalous thermal transport in Eshelby twisted van der Waals nanowires. *Nat. Mater.* **2025**, *24*, 728–734.
- (2) Zhang, C.; Sun, J.; Shen, Y.; Kang, W.; Wang, Q. Effect of high order phonon scattering on the thermal conductivity and its response to strain of a penta-NiN<sub>2</sub> sheet. *J. Phys. Chem. Lett.* **2022**, *13*, 5734–5741.
- (3) Liu, H.; Qin, G.; Lin, Y.; Hu, M. Disparate strain dependent thermal conductivity of two-dimensional penta-structures. *Nano Lett.* **2016**, *16*, 3831–3842.
- (4) Wu, X.; Han, Q. Phonon thermal transport across multilayer graphene/hexagonal boron nitride van der Waals heterostructures. *ACS Appl. Mater. Interfaces.* **2021**, *13*, 32564–32578.
- (5) Ding, W.; Ong, Z.-Y.; An, M.; Davier, B.; Hu, S.; Ohnishi, M.; Shiomi, J. Optimally suppressed phonon tunneling in van der Waals graphene–WS<sub>2</sub> heterostructure with ultralow thermal conductivity. *Nano Lett.* **2024**, *24*, 13754–13759.
- (6) Ouyang, W.; Qin, H.; Urbakh, M.; Hod, O. Controllable thermal conductivity in twisted homogeneous interfaces of graphene and hexagonal boron nitride. *Nano Lett.* **2020**, *20*, 7513–7518.
- (7) Cao, Y.; Fatemi, V.; Fang, S.; Watanabe, K.; Taniguchi, T.; Kaxiras, E.; Jarillo-Herrero, P. Unconventional superconductivity in magic-angle graphene superlattices. *Nature* **2018**, *556*, 43–50.
- (8) Park, J. M.; Cao, Y.; Watanabe, K.; Taniguchi, T.; Jarillo-Herrero, P. Tunable strongly coupled superconductivity in magic-angle twisted trilayer graphene. *Nature* **2021**, *590*, 249–255.
- (9) Zhang, C.; Sun, J.; Shen, Y.; Zhang, C.; Wang, Q.; Yoshikawa, A.; Kawazoe, Y.; Jena, P. Extremely large response of phonon coherence in twisted penta-NiN<sub>2</sub> bilayer. *Small* **2023**, *19*, No. 2303295.
- (10) Chen, Y.; Zhang, C.; Sun, J.; Ni, D.; Zhang, C.; Wang, Q. Tuning the lattice thermal conductivity of bilayer penta-graphene by interlayer twisting. *Appl. Surf. Sci.* **2023**, *635*, No. 157718.

- (11) Beltukov, Y.; Fusco, C.; Parshin, D.; Tanguy, A. Boson peak and Ioffe-Regel criterion in amorphous siliconlike materials: The effect of bond directionality. *Phys. Rev. E* **2016**, *93*, No. 023006.
- (12) Chumakov, A.; Sergueev, L.; Van Bürck, U.; Schirmacher, W.; Asthalter, T.; Rüffer, R.; Leupold, O.; Petry, W. Collective nature of the boson peak and universal transboson dynamics of glasses. *Phys. Rev. Lett.* **2004**, *92*, No. 245508.
- (13) Tømterud, M.; Eder, S. D.; Büchner, C.; Wondraczek, L.; Simonsen, I.; Schirmacher, W.; Manson, J. R.; Holst, B. Observation of the boson peak in a two-dimensional material. *Nat. Phys.* **2023**, *19*, 1910–1915.
- (14) Wu, J.; Lin, Y.; Shu, M.; Liu, Y.; Ma, Y.; Lin, G.; Zhang, C.; Jiao, P.; Zhu, F.; Wu, Y.; Ewings, R. A.; Walker, H. C.; Deng, G.; Chi, S.; Jiang, S.; Baggioli, M.; Jin, M.; Wang, H.; Xie, W.; Wei, T.-R.; Yang, J.; Shi, X.; Ma, J. Uncovering the phonon spectra and lattice dynamics of plastically deformable InSe van der Waals crystals. *Nat. Commun.* **2024**, *15*, 6248.
- (15) Schirmacher, W.; Ruocco, G.; Scopigno, T. Acoustic attenuation in glasses and its relation with the boson peak. *Phys. Rev. Lett.* **2007**, *98*, No. 025501.
- (16) Zhang, L.; Wang, Y.; Chen, Y.; Shang, J.; Sun, A.; Sun, X.; Yu, S.; Zheng, J.; Wang, Y.; Schirmacher, W.; Zhang, J. Disorder-induced vibrational anomalies from crystalline to amorphous solids. *Phys. Rev. Res.* **2021**, *3*, No. L032067.
- (17) Schirmacher, W.; Ruocco, G. Vibrational excitations in disordered solids. *Encyclopedia of Condensed-Matter Physics* **2024**, *5*, 298–317.
- (18) Sun, J.; Hu, M.; Zhang, C.; Bai, L.; Zhang, C.; Wang, Q. Ultralow thermal conductivity of layered Bi<sub>2</sub>O<sub>2</sub>Se induced by twisting. *Adv. Funct. Mater.* **2022**, *32*, No. 2209000.
- (19) Milkus, R.; Zacccone, A. Local inversion-symmetry breaking controls the boson peak in glasses and crystals. *Phys. Rev. B* **2016**, *93*, No. 094204.
- (20) Oyedele, A. D.; Yang, S.; Liang, L.; Puzos, A. A.; Wang, K.; Zhang, J.; Yu, P.; Pudasaini, P. R.; Ghosh, A. W.; Liu, Z.; Rouleau, C. M.; Sumpter, B. G.; Chisholm, M. F.; Zhou, W.; Rack, P. D.; Geohagan, D. B.; Xiao, K. PdSe<sub>2</sub>: pentagonal two-dimensional layers with high air stability for electronics. *J. Am. Chem. Soc.* **2017**, *139*, 14090–14097.
- (21) Chow, W. L.; Yu, P.; Liu, F.; Hong, J.; Wang, X.; Zeng, Q.; Hsu, C.-H.; Zhu, C.; Zhou, J.; Wang, X.; Xia, J.; Yan, J.; Chen, Y.; Wu, D.; Yu, T.; Shen, Z.; Lin, H.; Jin, C.; Tay, B. K.; Liu, Z. High mobility 2D palladium diselenide field-effect transistors with tunable ambipolar characteristics. *Adv. Mater.* **2017**, *29*, No. 1602969.
- (22) Zhao, Y.; Yu, P.; Zhang, G.; Sun, M.; Chi, D.; Hippalgaonkar, K.; Thong, J. T.; Wu, J. Low-symmetry PdSe<sub>2</sub> for high performance thermoelectric applications. *Adv. Funct. Mater.* **2020**, *30*, No. 2004896.
- (23) Wu, D.; Guo, J.; Du, J.; Xia, C.; Zeng, L.; Tian, Y.; Shi, Z.; Tian, Y.; Li, X. J.; Tsang, Y. H.; Jie, J. Highly polarization-sensitive, broadband, self-powered photodetector based on graphene/PdSe<sub>2</sub>/germanium heterojunction. *ACS Nano* **2019**, *13*, 9907–9917.
- (24) Jena, T.; Hossain, M. T.; Giri, P. Temperature-dependent Raman study and determination of anisotropy ratio and in-plane thermal conductivity of low-temperature CVD-grown PdSe<sub>2</sub> using unpolarized laser excitation. *J. Mater. Chem. C* **2021**, *9*, 16693–16708.
- (25) Yu, J.; Kuang, X.; Li, J.; Zhong, J.; Zeng, C.; Cao, L.; Liu, Z.; Zeng, Z.; Luo, Z.; He, T.; Pan, A.; Liu, Y. Giant nonlinear optical activity in two-dimensional palladium diselenide. *Nat. Commun.* **2021**, *12*, 1083.
- (26) Li, P.; Zhang, J.; Zhu, C.; Shen, W.; Hu, C.; Fu, W.; Yan, L.; Zhou, L.; Zheng, L.; Lei, H.; Liu, Z.; Zhao, W.; Gao, P.; Yu, P.; Yang, G. Penta-PdPSe: a new 2D pentagonal material with highly in-plane optical, electronic, and optoelectronic anisotropy. *Adv. Mater.* **2021**, *33*, No. 2102541.
- (27) Bykov, M.; Bykova, E.; Ponomareva, A. V.; Tasnadi, F.; Chariton, S.; Prakashenka, V. B.; Glazyrin, K.; Smith, J. S.; Mahmood, M. F.; Abrikosov, I. A.; et al. Realization of an ideal Cairo tessellation in nikel diazenide NiN<sub>2</sub>: high-pressure route to pentagonal 2D materials. *ACS Nano* **2021**, *15*, 13539–13546.
- (28) Liu, L.; Ji, Y.; Bianchi, M.; Hus, S. M.; Li, Z.; Balog, R.; Miwa, J. A.; Hofmann, P.; Li, A.-P.; Zemlyanov, D. Y.; Li, Y.; Chen, Y. P. A metastable pentagonal 2D material synthesized by symmetry-driven epitaxy. *Nat. Mater.* **2024**, *23*, 1339–1346.
- (29) Prasongkit, J.; Jungthawan, S.; Villagonzalo, C. D. Enhancing Thermoelectric efficiency in twisted bilayer PdSe<sub>2</sub>. *ACS Appl. Energy Mater.* **2024**, *7*, 7798–7807.
- (30) Fan, Z.; Dong, H.; Harju, A.; Ala-Nissila, T. Homogeneous nonequilibrium molecular dynamics method for heat transport and spectral decomposition with many-body potentials. *Phys. Rev. B* **2019**, *99*, No. 064308.
- (31) Fan, Z.; Zeng, Z.; Zhang, C.; Wang, Y.; Song, K.; Dong, H.; Chen, Y.; Ala-Nissila, T. Neuroevolution machine learning potentials: combining high accuracy and low cost in atomistic simulations and application to heat transport. *Phys. Rev. B* **2021**, *104*, No. 104309.
- (32) Carreras, A.; Togo, A.; Tanaka, I. DynaPhoPy: A code for extracting phonon quasiparticles from molecular dynamics simulations. *Comput. Phys. Commun.* **2017**, *221*, 221–234.
- (33) Larkin, J.; Turney, J.; Massicotte, A.; Amon, C.; McGaughey, A. Comparison and evaluation of spectral energy methods for predicting phonon properties. *J. Comput. Theor. Nanosci.* **2014**, *11*, 249–256.
- (34) Simoncelli, M.; Marzari, N.; Mauri, F. Wigner formulation of thermal transport in solids. *Phys. Rev. X* **2022**, *12*, No. 041011.
- (35) Lazić, P. CellMatch: Combining two unit cells into a common supercell with minimal strain. *Comput. Phys. Commun.* **2015**, *197*, 324–334.
- (36) Zhang, Y.; Tian, H.; Li, H.; Yoon, C.; Nelson, R. A.; Li, Z.; Watanabe, K.; Taniguchi, T.; Smirnov, D.; Kawakami, R. K.; Goldberger, J. E.; Zhang, F.; Lau, C. N. Quantum octets in high mobility pentagonal two-dimensional PdSe<sub>2</sub>. *Nat. Commun.* **2024**, *15*, 761.
- (37) Liu, X.; Peng, R.; Sun, Z.; Liu, J. Moiré phonons in magic-angle twisted bilayer graphene. *Nano Lett.* **2022**, *22*, 7791–7797.
- (38) Fan, Z.; Wang, Y.; Ying, P.; Song, K.; Wang, J.; Wang, Y.; Zeng, Z.; Xu, K.; Lindgren, E.; Rahm, J. M.; Gabourie, A. J.; Liu, J.; Dong, H.; Wu, J.; Chen, Y.; Zhong, Z.; Sun, J.; Erhart, P.; Su, Y.; Ala-Nissila, T. GPUMD: a package for constructing accurate machine-learned potentials and performing highly efficient atomistic simulations. *J. Chem. Phys.* **2022**, *157*, No. 114801.
- (39) Fan, Z. Improving the accuracy of the neuroevolution machine learning potential for multi-component systems. *J. Phys.: Condens. Matter* **2022**, *34*, No. 125902.
- (40) Chen, L.; Zhang, W.; Zhang, H.; Chen, J.; Tan, C.; Yin, S.; Li, G.; Zhang, Y.; Gong, P.; Li, L. In-plane anisotropic thermal conductivity of low-symmetry PdSe<sub>2</sub>. *Sustainability* **2021**, *13*, 4155.
- (41) Simoncelli, M.; Marzari, N.; Mauri, F. Unified theory of thermal transport in crystals and glasses. *Nat. Phys.* **2019**, *15*, 809–813.
- (42) Zhang, C.; Sun, J.; Cheng, J.; Wang, Q. Ultralow lattice thermal conductivity in quasi-one-dimensional BiI<sub>3</sub> with suppressed phonon coherence. *Phys. Rev. B* **2024**, *110*, No. 174309.
- (43) Keune, W.; Hong, S.; Hu, M. Y.; Zhao, J.; Toellner, T.; Alp, E. E.; Sturhahn, W.; Rahman, T.; Roldan Cuenya, B. Influence of interfaces on the phonon density of states of nanoscale metallic multilayers: phonon confinement and localization. *Phys. Rev. B* **2018**, *98*, No. 024308.
- (44) Yang, L.; Yang, N.; Li, B. Reduction of thermal conductivity by nanoscale 3D phononic crystal. *Sci. Rep.* **2013**, *3*, 1143.
- (45) Hu, Y.-C.; Tanaka, H. Origin of the boson peak in amorphous solids. *Nat. Phys.* **2022**, *18*, 669–677.
- (46) Ren, S.; Zong, H.-X.; Tao, X.-F.; Sun, Y.-H.; Sun, B.-A.; Xue, D.-Z.; Ding, X.-D.; Wang, W.-H. Boson-peak-like anomaly caused by transverse phonon softening in strain glass. *Nat. Commun.* **2021**, *12*, 5755.
- (47) Thompson, A. P.; Aktulga, H. M.; Berger, R.; Bolintineanu, D. S.; Brown, W. M.; Crozier, P. S.; in 't Veld, P. J.; Kohlmeyer, A.; Moore, S. G.; Nguyen, T. D.; Shan, R.; Stevens, M. J.; Tranchida, J.; Trott, C.; Plimpton, S. J. LAMMPS—a flexible simulation tool for

particle-based materials modeling at the atomic, meso, and continuum scales. *Comput. Phys. Commun.* **2022**, *271*, No. 108171.

(48) Ioffe, A.; Regel, A. Non-crystalline, amorphous, and liquid electronic semiconductors. *Prog. Semicond.* **1960**, *4*, 237–291.